Analysis of Millimeter Wave Phase Shifters Coupled to a Fixed Periodic Structure

Jin Liu, Jerome K. Butler, *Fellow, IEEE*, Gary A. Evans, *Fellow, IEEE*, and Arye Rosen, *Fellow, IEEE*

***Abstract*—The propagation characteristics of an active plasma-induced millimeter wave phase shifter coupled to a fixed periodic structure are discussed. The numerical calculation is based on an improved boundary value solution. Like a normal dielectric slab waveguide with a plasma layer, the grating waveguide displays a phase shift with the increase of the plasma density. This phase shift due to the significant change of the field distribution has an impact on the modal attenuation coefficient. It results in the scanning of the radiation beam in the vicinity of the second Bragg. Especially, at both weak and strong plasma densities when the mode losses are small, the resonances caused by the periodic structure do not appear to be weakened. The results can be used to design electronically controllable millimeter wave scanning antennas.**

I. Introduction

PERIODIC STRUCTURES have been used in the design of millimeter waveguide antennas because of their special propagation characteristics in the vicinity of the Bragg resonances [1], [2]. A simple way to introduce periodicity is to incorporate a grating at a dielectric interface. The grating structure can produce broadside radiation in the transverse direction, and contra-directional mode-coupling [3] in the vicinity of the second Bragg. In some applications it is desirable to scan the beam. However, beam scanning with a fixed grating period requires a change in the source frequency, or the effective index of the propagating mode. An adjustable propagation constant by using optical radiation has been reported [4] and demonstrated on silicon waveguides by using the free carrier effects of the semiconductor material to modify the electric permittivity. Such a beam-steerable semiconductor waveguide antenna with metal grating teeth has been developed [5]–[7]. A numerical analysis of the light induced grating structure was also developed [8].

The mechanism of a beam-steerable waveguide antenna is based on the fact that the complex dielectric constant of a semiconductor material such as silicon, is changed when incident light photons generate electron-hole pairs producing a plasma. The number of electron-hole pairs generate a plasma density N inside the semiconductor that is proportional to the incident light intensity I that can be expressed as, [8]

$$I = \frac{\hbar\omega_L N t_p}{(1-R)\eta\tau_0} \propto N t_p \tag{1}$$

where t_p is the thickness of the semiconductor layer, ω_L the angular frequency of the light, R the reflectivity of the light at the semiconductor surface, η the quantum efficiency of the semiconductor layer, N is the excess electron-hole density, and τ_0 the life time of the carriers. According to the Drude–Lorentz theory [9], the complex dielectric constant can be written as [4]

$$\epsilon(\omega, N) = \epsilon_r - \sum_i \frac{\omega_{pi}^2}{\omega^2 + \nu_i^2} - \frac{j}{\omega}\sum_i \frac{\omega_{pi}^2 \nu_i}{\omega^2 + \nu_i^2} \tag{2}$$

where ϵ_r is the dielectric constant of the passive semiconductor material, ω the frequency of the propagating wave, ω_{pi} the plasma frequency, and ν_i relaxation frequency of the ith carrier. Expressing the dielectric constant as $n - jk = \sqrt{\epsilon(\omega, N)}$, we may conclude that both refractive index n and extinction coefficient k increase with the plasma density, and the extinction coefficient may exceed the refractive index for high values of the plasma density N [4]. At a high plasma density, the semiconductor layer shows a strong metallic characteristic.

Regarding the dielectric slab waveguide with a plasma layer [10], it was found that the phase changed with increasing plasma density. The phase shift was due to the change of the propagation constant when the dielectric property of the plasma layer changed from lightly absorbing to metallic; this resulted in a significant difference between the field distributions at a low plasma density and that at a high plasma density. Because of the difference between the TE mode and TM mode field distributions, the phase shifts of TE and TM modes are in the opposite directions. In addition to the change of the propagation constant, there is also a strong modification of the wave attenuation [10]. At low plasma densities, the attenuation coefficient is proportional to the imaginary part of the refractive index, and it increases with the plasma density. However, the attenuation is saturated and reaches a maximum value, when the metallic characteristic of the plasma layer becomes increasingly significant and causes the highest loss of propagating power. Then, with the plasma density reaching a higher level, the attenuation coefficient decreases, and the plasma layer actually becomes a metallic thin film.

In this paper, our focus is on a rigorous numerical analysis of the propagation and radiation characteristics of a millimeter waveguide with a fixed dielectric grating structure coated with a light-induced plasma layer on the surface opposite to the grating layer, shown in Fig. 1. This configuration of the millimeter waveguide will have the second Bragg condition occurring at 95 GHz. The lateral width of the waveguide is assumed to be infinite with no variation in the y-direction.

Manuscript received June 29, 1995; revised April 19, 1996.

J. Liu, J. K. Butler, and G. A. Evans are with the Department of Electrical Engineering, Southern Methodist University, Dallas, TX 75275-0338 USA.

A. Rosen is with the David Sarnoff Research Center, Princeton, NJ 08543-0335 USA.

Publisher Item Identifier S 0018-9480(96)05652-9.

0018–9480/96$05.00 © 1996 IEEE

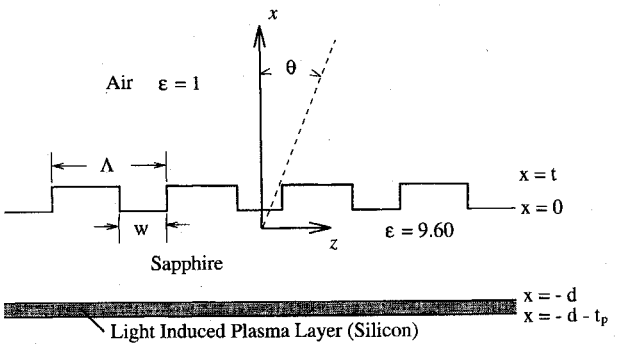

Fig. 1. The configuration of the millimeter wave phase shifter with rectangular grating profile. The grating period $\Lambda = 1333$ μm, grating tooth gap $w = 600$ μm, grating layer thickness $t = 180$ μm, guiding layer thickness $d = 800$ μm, and plasma layer thickness $t_p = 0.01$ μm $- 50$ μm.

The actual expression for the field distribution in a periodic waveguide is obtained using the Floquet-Bloch expansion as a solution of the wave equation. At Bragg resonances there is a strong interaction between two major spatial harmonics that have the appearance of "propagating" in opposite directions. This phenomena is especially true in the vicinity of the second Bragg condition (the fast wave region). The spatial harmonic $n = -1$ with a relatively small axial propagation constant, causes significant propagation in the transverse direction, so that the periodic waveguide exhibits radiation [11]. The direction of the radiated beam is tied to the value of the propagation constant, and will be shifted or scanned due to the change of the propagation constant. If the periodic waveguide has a light induced plasma layer with a controllable dielectric constant, it can produce surface emission with an adjustable radiation pattern. It is noted that at both high and low plasma densities, the ohmic loss is negligible, and the Bragg resonances are clearly visible from the $\omega - \beta$ dispersion curve. In our study, the plasma density is assumed to be uniform throughout the layer. By using a transfer matrix method, the boundary conditions at the interfaces of the grating region may be obtained. The solution in the grating region is based on the method proposed by Chang *et al.* [12]. However, for the calculations discussed in the paper, the single step implicit Runge-Kutta method is used as opposed to the multistep formulation to solve the differential equations. With this algorithm, the computing is more efficient, and the accuracy and stability are improved.

We consider a thick sapphire waveguide with a rectangular grating at the sapphire air ($\epsilon_g = 9.6, \epsilon_a = 1.0$) interface of thickness $t = 180$ μm, as shown in Fig. 1. The bottom of the waveguide has a thin silicon layer. Its thickness t_p ranges from 0.01 to 50 μm and is less than 10% of the waveguide thickness. The grating period of the waveguide is $\Lambda = 1.333$ mm, the distance between the grating teeth $w = 0.6$ mm, and the guiding layer thickness is 0.8 mm.

II. Numerical Foundation

Frequently, modes in periodic structures are intuitively visualized using approximate methods such as the coupled-mode formulation where the fields are described by the superposition of the backward and forward waves. However, an accurate solution of the periodic waveguide is based on the Floquet–Bloch theory. The field in a periodic waveguide can be expressed in terms of the Floquet–Bloch functions

$$\Psi(\boldsymbol{r}) = \sum_{n=-\infty}^{\infty} \Psi_n(x) e^{-\gamma_n z} \tag{3}$$

where

$$\gamma_n = \alpha + j(\beta + nK). \tag{4}$$

β and α are the propagation and attenuation constants respectively. Each term in (3) is called a *spatial harmonic*. Usually, the $n = 0$ guiding spatial harmonic is dominant. However, some harmonics may have relatively large amplitudes if there is strong interaction with another harmonic [1]. In the periodic waveguide, multiple guided modes may be excited. If the propagation constant of the pth guided mode is denoted as $\beta^{(p)}$, then a resonance occurs provided

$$\beta^{(p)} + \beta^{(q)} = lK, \qquad l, p, q = 1, 2, 3, \cdots. \tag{5}$$

Modes operating near the second Bragg ($l = 2$) are useful for surface emitting devices, because the $n = -1$ spatial harmonic with a small longitudinal propagation constant becomes an outward leaky wave.

There are many methods that can be used to solve the periodic waveguide problem, such as the coupled-mode theory [13], [14], perturbation techniques [15], [16], boundary-value methods [12], and eigensystem methods [17]. The boundary-value approach is an effective method used to analyze the propagation characteristics. In this formulation it is assumed that there is no y-dependence in the field distributions. Accordingly, the only field components are E_y, H_x, H_z for TE modes and H_y, E_x, E_z for TM modes. In the grating region, the electric permittivity can be written as a function of both x and z, and Maxwell's equations become a set of first order partial differential equations. The periodic permittivity function and its inverse in the grating region can be expanded in a Fourier series so that, with (3) and normalized notation for the electromagnetic fields

$$\Psi = \begin{cases} E_y & \text{TE mode} \\ H_y & \text{TM mode} \end{cases}, \qquad \Phi = \begin{cases} \sqrt{\dfrac{\mu_0}{\epsilon_0}} H_z & \text{TE mode} \\ \sqrt{\dfrac{\epsilon_0}{\mu_0}} E_z & \text{TM mode} \end{cases} \tag{6}$$

and we can discretize Maxwell's equations as

$$\begin{aligned} \frac{d\boldsymbol{\Psi}(x)}{dx} &= \boldsymbol{U}(x)\boldsymbol{\Phi}(x) \\ \frac{d\boldsymbol{\Phi}(x)}{dx} &= \boldsymbol{V}(x)\boldsymbol{\Psi}(x). \end{aligned} \tag{7}$$

$\boldsymbol{U}(x)$ and $\boldsymbol{V}(x)$ are square matrices whose elements are functions of the propagation constant and the Fourier coefficients of the periodic permittivity in the grating region [12]. $\boldsymbol{\Psi}(x)$ and $\boldsymbol{\Phi}(x)$ are column vectors with elements $\Psi_n(x)$ and $\Phi_n(x)$, respectively.

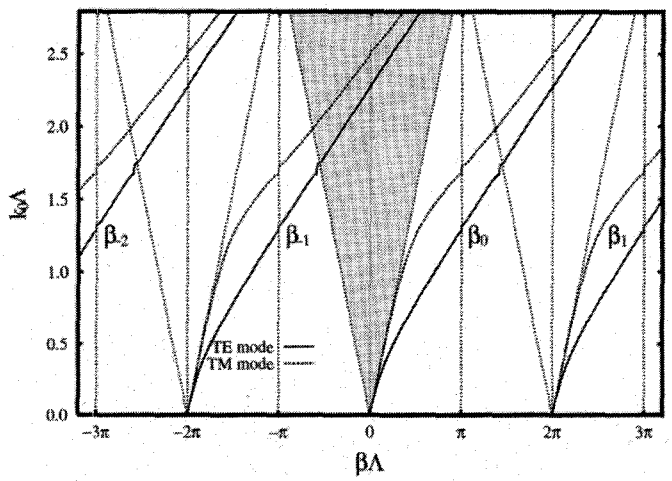

Fig. 2. The $k_0\Lambda$-$\beta\Lambda$ plot. The shadowed area is the fast wave region.

Alternatively, the above equation may be rewritten in an integrated form as

$$\boldsymbol{Y}'(x) = \boldsymbol{F}(x)\boldsymbol{Y}(x) \tag{8}$$

where

$$\boldsymbol{Y}(x) = \begin{bmatrix} \boldsymbol{\Psi}(x) \\ \boldsymbol{\Phi}(x) \end{bmatrix}, \quad \boldsymbol{F}(x) = \begin{bmatrix} 0 & \boldsymbol{U}(x) \\ \boldsymbol{V}(x) & 0 \end{bmatrix}. \tag{9}$$

$\boldsymbol{F}(x)$ in (8) represents the coupling between the spatial harmonics due to the periodic structure. The field of each spatial harmonic n in the other uniform layers can be expressed in a plane wave form

$$\Psi_n(x) = A_n \cos(h_n x) + B_n \sin(h_n x) \tag{10}$$

where the transverse wave vector

$$h_n = \pm\sqrt{\epsilon k_0^2 + \gamma_n^2} \tag{11}$$

and ϵ is the permittivity of the dielectric layer. The sign of h_n is chosen to obtain an outward transverse wave in the superstrate and substrate. The outward transverse wave in the superstrate and substrate also enable us to derive the relation between $\Psi_n(x)$ and its derivative at the interfaces of the grating layer. In a multiple layer system, the transfer matrix method is an effective way to obtain such relations that actually become the homogeneous boundary conditions of the differential equations given by (7) in [12]

$$\begin{aligned} \boldsymbol{R}(t)\frac{d\boldsymbol{\Psi}(t)}{dx} + \boldsymbol{S}(t)\boldsymbol{\Psi}(t) &= 0 \\ \boldsymbol{R}(0)\frac{d\boldsymbol{\Psi}(0)}{dx} + \boldsymbol{S}(0)\boldsymbol{\Psi}(0) &= 0 \end{aligned} \tag{12}$$

where t is the grating layer thickness, as shown in Fig. 1. The elements in the square matrices $\boldsymbol{R}(x)$ and $\boldsymbol{S}(x)$ are related to the parameters of the multiple dielectric layer structure, such as, the layer thickness, permittivities, and the propagation constant β and attenuation constant α.

To solve (8), the square matrices are truncated, and only a finite number of the spatial harmonics are used since spatial harmonics with large $|n|$ values have negligible contributions to the field distribution. In general, for the linear equation

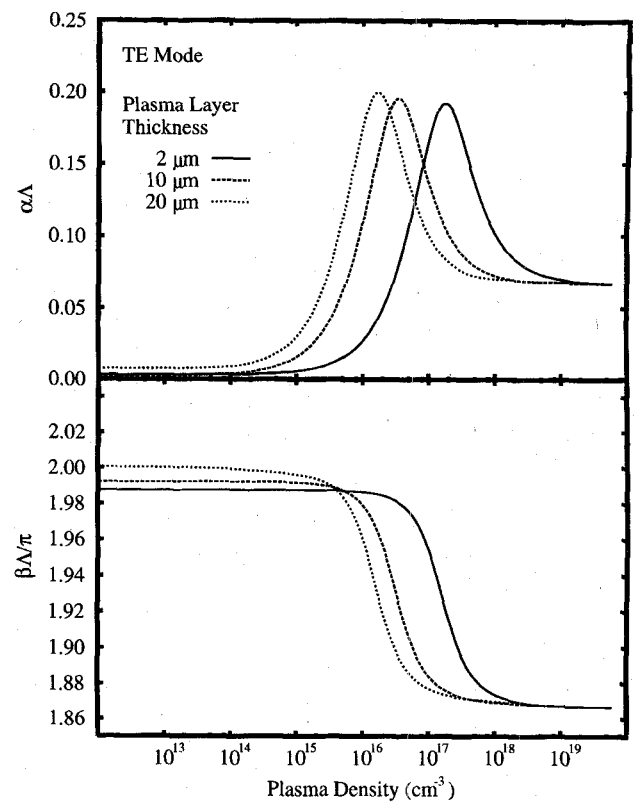

Fig. 3. The propagation and attenuation properties for TE modes in the waveguide with a rectangular grating profile and a source frequency of 81.3 GHz ($k_0\Lambda = 2.27$).

$y' = f(x)y$, the fourth-order implicit Runge–Kutta formula can be reduced into an explicit one to avoid time consuming iterations. To apply the Runge–Kutta formula, the grating region may be divided equally into n intervals. Generally, the solution at x_{i+1} can be expressed in terms of that at x_i as

$$\begin{aligned} \boldsymbol{Y}(x_{i+1}) &= [1 + \boldsymbol{G}_i(x_i)h]\boldsymbol{Y}(x_i), \qquad i = 0, 1, 2, \cdots, n, \\ x_0 &= 0, \cdots, x_n = t \end{aligned} \tag{13}$$

where h is the thickness of each interval. The function $\boldsymbol{G}_i(x_i)$ is determined by the numerical formulation and the characteristics of each interval.

Combining (13), (12), and (7) a set of homogeneous linear equations can be derived as

$$\mathcal{M}(\gamma)\boldsymbol{Y}(0) = 0 \tag{14}$$

where $\mathcal{M}$ is a matrix which can be described by matrices $\boldsymbol{R}(x), \boldsymbol{S}(x), \boldsymbol{U}(x), \boldsymbol{V}(x)$, and $\boldsymbol{G}(x)$. The nontrivial solution of $\boldsymbol{Y}(0)$ can be obtained under the condition

$$\det|\mathcal{M}(\gamma)| = 0. \tag{15}$$

This secular equation must be satisfied by the complex propagation constant $\gamma = \alpha + j\beta$, and it is solved for roots using the Muller method. Since the formulation is analytically based, the numerical error is mainly caused by the truncation of the matrices and the number of intervals of the grating layer. It was found that 11–17 spatial harmonics are sufficient for the periodic millimeter waveguide with a strong grating. The number of intervals in the grating region depends on the accuracy

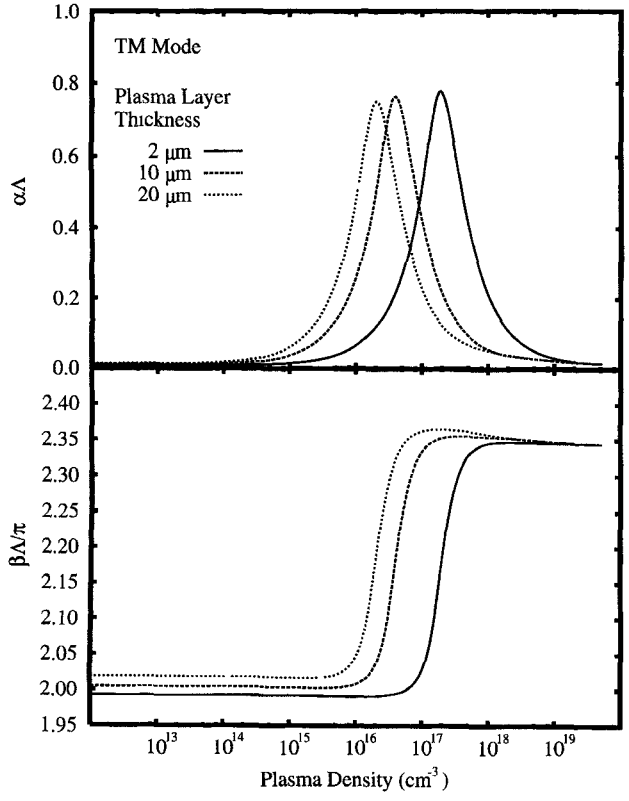

Fig. 4. The propagation and attenuation constants for TM modes in the waveguide with a rectangular grating profile and a source frequency of 91.3 GHz ($k_0\Lambda = 2.55$).

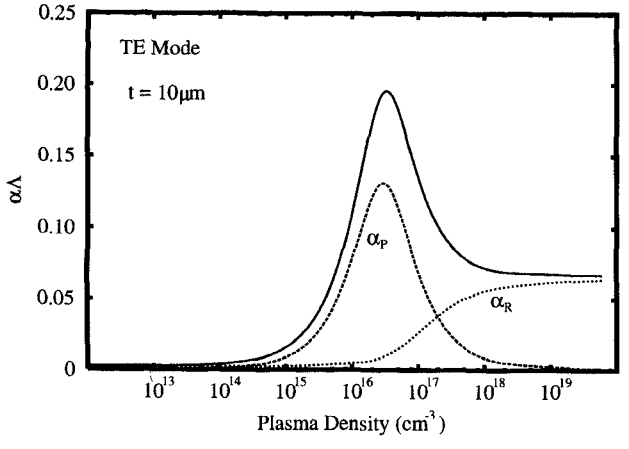

Fig. 5. Comparison of the attenuation characteristics for the TE mode. α_P is due to the plasma layer; α_R is the attenuation only caused by the periodic structure; α includes both loss mechanisms.

of the numerical method for solving the differential equation. By using 100–200 intervals in the grating layer, satisfactory results can be obtained for the fourth order formulation.

III. Propagation Characteristics

The grating waveguide exhibits Bragg resonances with significant attenuation due to radiation at operating frequencies in the vicinity of the second Bragg condition. Such radiation is caused by the $n = -1$ spatial harmonic that has a small longitudinal propagation constant. If the $n = -1$ harmonic is

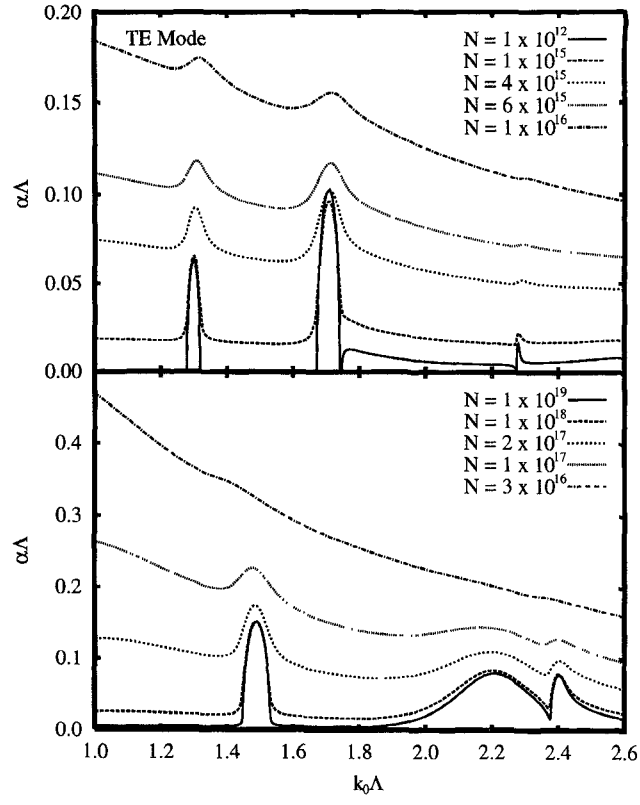

Fig. 6. The attenuation constant for the TE modes in the waveguide as a function of the source wave vector $k_0\Lambda$ with different plasma densities.

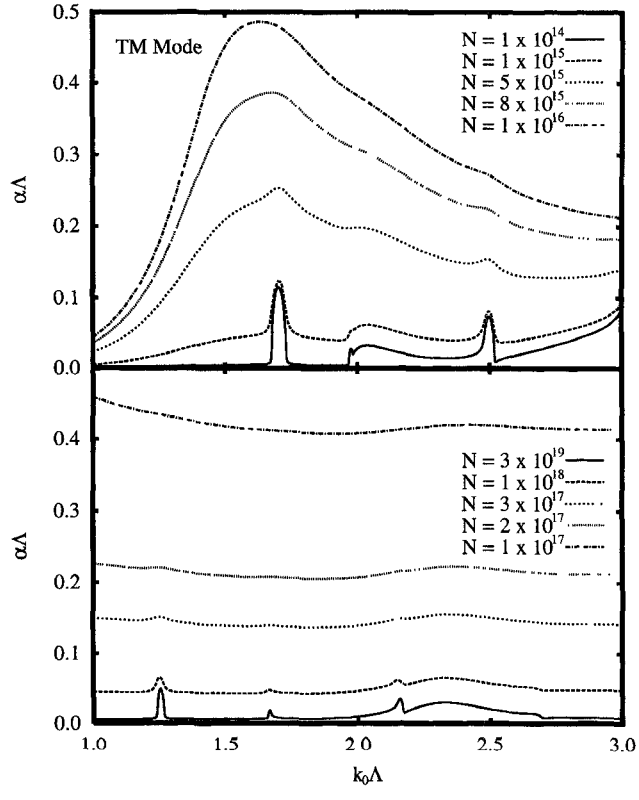

Fig. 7. The attenuation constant for the TM modes in the waveguide as a function of the source wave vector $k_0\Lambda$ with different plasma densities.

treated as a component wave, in the view of ray optics, the angle θ of the propagation direction of the spatial harmonic to

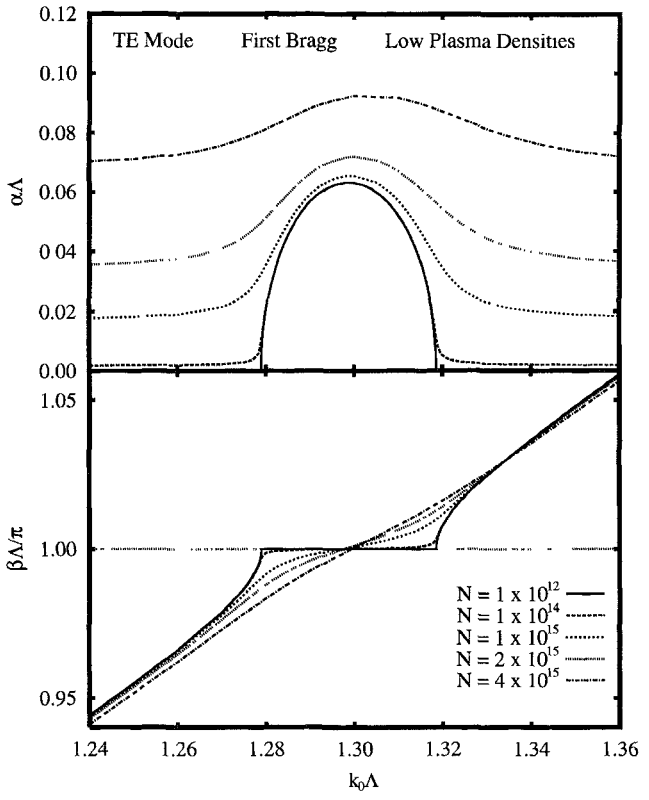

Fig. 8. The propagation and attenuation constants for the TE modes in the waveguide as the function of the source wave vector $k_0\Lambda$ in the vicinity of the first Bragg under different plasma densities.

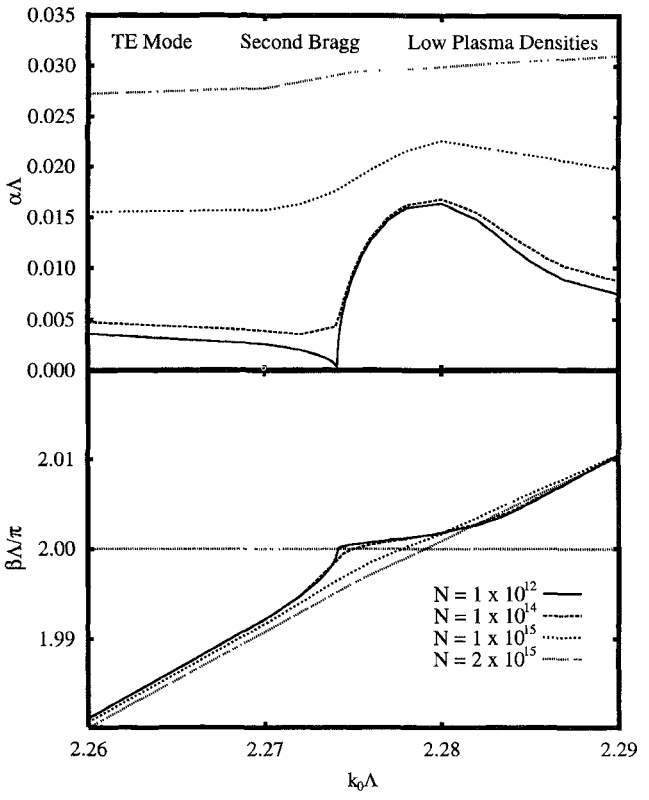

Fig. 9. The propagation and attenuation constants for the TE modes in the waveguide as the function of the source wave vector $k_0\Lambda$ in the vicinity of the first Bragg under different plasma densities.

the normal direction is, shown in Fig. 1

$$\theta = \tan^{-1}\mathrm{Re}\left(\frac{h_{-1}}{\gamma_{-1}}\right) = \tan^{-1}\left(\frac{\mathrm{Re}(h_{-1})}{\beta - K}\right) = \sin^{-1}\left(\frac{\beta - K}{n_r k_0}\right) \tag{16}$$

where h_{-1} is the transverse wavevector of the $n = -1$ spatial harmonic

$$h_{-1} = \pm\sqrt{\epsilon k_0^2 + \gamma_{-1}^2} \tag{17}$$

ϵ is the permittivity of the propagation media, and $n_r = \sqrt{\epsilon}$ is the corresponding refractive index. The condition of the $n = -1$ spatial harmonic propagating in air superstrate and air substrate is

$$\left|\frac{\beta - K}{k_0}\right| < 1. \tag{18}$$

In the superstrate or the substrate of the waveguide, if there is a wave propagating in the direction which is not parallel to the longitudinal direction, i.e., $|\theta| < 90°$, then the electromagnetic energy will be leaked or radiated from the waveguide to the surrounding media. On the other hand, if

$$\left|\frac{\beta - K}{k_0}\right| \geq 1 \tag{19}$$

then total internal reflection will occur at the boundaries of the waveguide, and the propagating wave will be "confined" to the waveguide. According to (18) we can draw boundaries in the dispersion diagram as shown in Fig. 2. In the shadowed area, called the fast wave region, the radiated power and the attenuation coefficient α become nonzero.

The propagation characteristics are examined as a function of the plasma density. The curves in Figs. 3 and 4 display many similarities to Figs. 2, 3, 6, and 7 of [10]. However, the phase shift results in the rotation of the outward radiation beam in the vicinity of the second Bragg. From (16), the shift of the radiation angle can be expressed as

$$\Delta\theta \approx \frac{\Delta\beta}{k_0}. \tag{20}$$

From Figs. 3 and 4, it can be estimated that the changes of the radiation angle are $-9.5°$ and $25.5°$ for TE and TM modes, respectively, when the plasma density increases from very low ($N < 10^{14}$ cm^{-3}) to very high ($N > 10^{18}$ cm^{-3}). The sign of $\Delta\theta$ indicates the direction of beam scanning with increase of the plasma density, which is clockwise for the TE mode, and counter clockwise for the TM mode, respectively. It is noted that the curves of the propagation constant and the attenuation coefficient retain shapes similar to those of the waveguide without a grating layer. The reason is that the $n = 0$ guiding spatial harmonic is basically dominant when the propagation constant of the periodic waveguide is off resonance. Because of the weak coupling between spatial harmonics, the propagation constant is very close to that of the waveguide with the grating layer replaced by a dielectric layer whose permittivity is equal to the mean value of that in the grating layer. However, the grating does have a significant

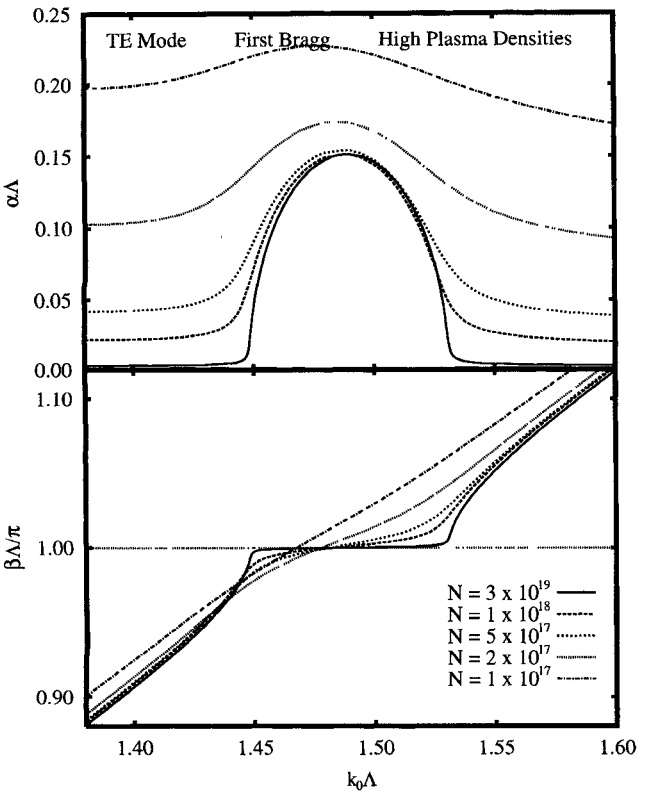

Fig. 10. The propagation and attenuation constants for the TE mode in the waveguide as the function of the source wave vector $k_0\Lambda$ in the vicinity of the second Bragg under different plasma densities.

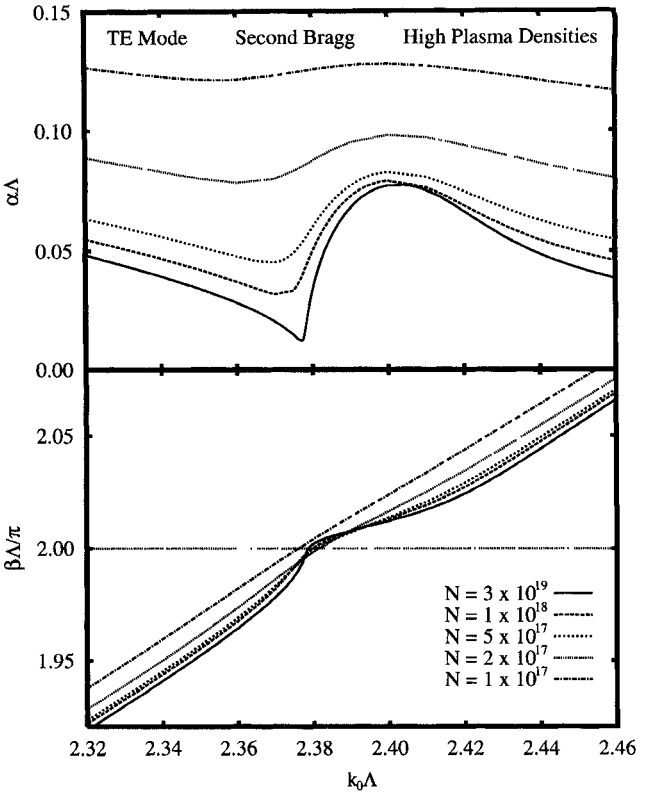

Fig. 11. The propagation and attenuation constants for the TE mode in the waveguide as the function of the source wave vector $k_0\Lambda$ in the vicinity of the second Bragg under different plasma densities.

impact on the attenuation coefficient. As shown in Figs. 3 and 5, the attenuation coefficient at high plasma levels is not as small as in the case of the same waveguide without any grating structure. This extra attenuation is contributed by the radiation power loss, because the shift of the propagation constant results in higher radiation loss in this particular situation.

To further analyze the attenuation, we recall that there are two types of power loss in the waveguide: dissipation in the plasma layer and radiation. Emission power is proportional to the guided power, and the $n = -1$ spatial harmonic can be considered as the only term responsible for the radiation in the vicinity of the second Bragg, since it has the largest longitudinal propagation constant among the other spatial harmonics. Accordingly, the amplitude of the attenuation coefficient contribution from the outgoing $n = -1$ spatial harmonic may be defined as [16]

$$\alpha_R = \frac{\mathrm{Re}\{h_0|\Psi_{-1}(t)|^2 + h_0|\Psi_{-1}(-t_p - d)|^2\}}{2\beta\int_{-\infty}^{\infty}|\Psi_0(x)|^2\,dx}. \qquad (21)$$

The plasma layer has an ohmic power loss α_P in the absence of a grating. To compare the contributions to the attenuation from the plasma layer and from the periodic structure, α_P and α_R are evaluated numerically, shown in Fig. 5. α_P is the attenuation coefficient of a waveguide with the same configuration as shown in Fig. 1, except the grating layer is replaced by a uniform layer with an average permittivity value equal to $\epsilon_g D + \epsilon_0(1 - D)$ where the duty cycle $D = 1 - w/\Lambda$. α_R is the attenuation coefficient of a waveguide with the same configuration without the thin plasma layer. α_P and α_R are the attenuation coefficient caused by the plasma layer and the radiation, respectively. Additionally, the total α obtained previously includes contributions from the plasma layer and the grating. It is clear that $\alpha \approx \alpha_P + \alpha_R$ as shown in Fig. 5. This reveals that the attenuation due to the presence of the plasma layer is small at very low and very high plasma densities, and the attenuation is mainly due to the radiation power loss. At some intermediate level of plasma density, the attenuation caused by the plasma ohmic losses reaches maximum, and the guided power is highly dissipated, while the radiation power loss is almost unaffected.

The overall attenuation constants near the first and second Bragg conditions are shown in Figs. 6 and 7, as a function of the plasma density $N(\mathrm{cm}^{-3})$. The details of the TE mode in the vicinity of the first and second Bragg are shown in Figs. 8–11. These curves indicate that the fine structures of the Bragg resonances can not be observed because the highly absorbing plasma layer results in a much larger attenuation coefficient. However, at very high plasma densities, those resonances appear again in the attenuation and propagation curves. Another interesting phenomenon is that there are extra resonances between the first Bragg and the boundary of the fast wave region, for both TE and TM modes, as shown in Fig. 6. Numerical calculations show that the resonances are caused by the coupling between the spatial harmonics associated with the fundamental guided mode and the second guided mode, *i.e.* $p = 1, q = 2, l = 1$ in (5). However, at a high plasma density, the resonance disappears from the attenuation curve in Fig. 6

of the TE mode, while the resonance remains for the TM mode, despite its shape. The disappearance of the resonance occurs because the waveguide at high plasma density no longer supports the second guided mode at the frequency considered. This can also be explained by noting that the cut-off frequency of the waveguide becomes higher for the TE mode, and lower for the TM mode with the increase of the plasma density.

IV. Conclusion

The propagation characteristics of a waveguide with a fixed grating and a light-induced plasma layer has been presented. In the vicinity of the first Bragg resonance, the interaction between the spatial harmonics -1 and zero produces a high attenuation of the propagating wave. Here, the periodic waveguide appears as a wave reflector or contra directional mode coupler. However, with an increase in plasma density, the shift of the propagation constant may causes the first Bragg to move away from resonance, resulting in propagation through the waveguide with minor loss. By using this mechanism, it is possible to develop an optical fast switch to control the electromagnetic power propagation in the millimeter waveguide. If the first Bragg condition is used to design a band reject filter, the width and center frequency of the stop band can be adjustable. In the vicinity of the second Bragg which is inside the fast wave region, the periodic waveguide radiates power. The light induced plasma layer can steer the radiation beam. Particularly, at both high and low plasma densities, the internal ohmic heating in the plasma layer is inconsequential. Accordingly, the waveguide losses will be minimized, and the sharp effects of the Bragg resonances are present.

The characteristics of the periodic waveguide described in this paper have a common behavior that is exhibited by other periodic waveguides. The impact of the optically controlled plasma layer on the propagation and attenuation constants can help in the development of various optically-controllable millimeter wave devices.

References

[1] C. Elachi and C. Yeh, "Periodic structures in integrated optics," *J. Appl. Phys.*, vol. 44, no. 7, pp. 3146, 1973.

[2] J. Jacobsen, "Analytica, numerical, and experimental investigation of guided waves on a periodically strip-loaded dielectric slab," *IEEE Trans. Antennas and Propagation*, vol. AP-18, no. 3, pp. 379–387, 1970.

[3] G. A. Evans, "Electromagnetic theory of distributed feedback lasers in periodic dielectric waveguides," Ph.D. dissertation, CA Inst. Technol., Pasadena, CA, Sept. 1974.

[4] C. H. Lee, P. S. Mak, and A. P. DeFonzo, "Optical control of millimeter-wave propagation in dielectric waveguides," *IEEE J. Quant. Elect.*, vol. 16, no. 3, pp. 277–288, 1980.

[5] R. E. Horn, H. Jacobs, E. Freibergs, and K. L. Klohn, "Electronic modulated beam-steerable silicon waveguide array antenna," *IEEE Trans. Microwave Theory Tech.*, vol. MTT-28, no. 6, pp. 647–653, 1980.

[6] A. Rosen, R. Amantea, P. J. Stabile, A. E. Fathy, D. B. Gilbert, D. W. Bechtle, W. M. Janton, F. J. McGinty, J. K. Butler, and G. A. Evans, "Investigation of active antenna arrays at 60 GHz," *IEEE Trans. Microwave Theory Tech.*, vol. 43, no. 9, pp. 2117–2125, 1995.

[7] V. A. Manasson, L. S. Sadovnik, A. Moussessian, and D. B. Rutledge, "Millimeter-wave diffraction by a photo-induced plasma grating," *IEEE Trans. Microwave Theory Tech.*, vol. 43, no. 9, pp. 2288–2290, 1995.

[8] M. Matsumoto, M. Tsutsumi, and N. Kumagai, "Radiation of millimeter waves from a leaky dielectric waveguide with a light-induced grating layer," *IEEE Trans. Microwave Theory Tech.*, vol. MTT-35, no. 11, pp. 1033–1042, 1987.

[9] N. W. Ashcroft and N. D. Mermin, *Solid State Physics*. Philadelphia: W. B. Saunders, 1976, pp. 1–25.

[10] J. K. Butler, T. F. Wu, and M. W. Scott, "Nonuniform layer model of a millimeter-wave phase shifter," *IEEE Trans. Microwave Theory Tech.*, vol. MTT-34, no. 1, pp. 147–155, 1986.

[11] G. Hadjicostas, J. K. Butler, G. A. Evans, N. W. Carlson, and R. Amantea, "A numerical investigation of wave interactions in dielectric waveguides with periodic surface corrugations," *IEEE J. Quant. Elect.*, vol. 26, no. 5, pp. 893–902, 1990.

[12] K. C. Chang, V. Shah, and T. Tamir, "Scattering and guiding of waves by dielectric gratings with arbitrary profiles," *J. Opt. Soc. Am.*, vol. 70, no. 7, pp. 804–813, 1980.

[13] H. Kogelnik and C. V. Shank, "Coupled-wave theory of distributed feedback lasers," *J. Appl. Phys.*, vol. 43, no. 5, pp. 2327–2335, 1972.

[14] C. Elachi, Gary Evans, and C. Yeh, "Transversely bounded DFB lasers," *J. Opt. Soc. Am.*, vol. 65, no. 4, pp. 404–412, 1975.

[15] K. Handa, S. T. Peng, and T. Tamir, "Improved perturbation analysis of dielectric gratings," *Appl. Physics*, vol. 5, pp. 325–328, 1975.

[16] W. Streifer, D. R. Scrifres, and R. D. Burnham, "Analysis of grating-coupled radiation in GaAs:GaAlAs lasers and waveguides," *IEEE J. Quant. Elect.*, vol. QE-12, no. 7, pp. 422–428, 1976.

[17] S. T. Peng, T. Tamir, and H. L. Bertoni, "Theory of periodic dielectric waveguides," *IEEE Trans. Microwave Theory Tech.*, vol. MTT-23, pp. 123–133, 1976.

Jin Liu received the B.S. degree in physics from Fudan University, Shanghai, China, and the M.S. degree in physics from Texas A&M University, College Station, TX, and the Ph.D. degree in applied science from Southern Methodist University, Dallas, Texas, in 1984, 1991, and 1995, respectively.

From 1984 to 1988, he worked as a Teaching and Research Assistant in the Department of Physics, Fudan University. He is involved in the research on thin film and surface physics. From 1989 to 1991, he was a Teaching and Research Assistant at Texas A&M University. His research area was condense matter physics. From 1991 to 1994, he was a Research Assistant in the Department of Electrical Engineering, Southern Methodist University. He primarily worked on the numerical analysis of dielectric waveguides with periodic structures, especially the millimeter waveguides with surface corrugations, grating surface emitting laser and other semiconductor lasers. In 1995, he joined Aspen Technology Inc. (formerly Dynamic Matrix Control Corporation), Houston, TX. As a Senior Engineer, he is responsible for developing engineering softwares.

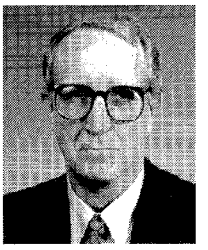

Jerome K. Butler (S'59–M'65–SM'78–F'89) was born in Shreveport, LA. He received the B.S.E.E. degree from Louisiana Polytechnic Institute, Ruston, in 1960, and the M.S.E.E. and Ph.D. degrees from the University of Kansas, Lawrence, in 1962 and 1965, respectively.

From 1960 to 1965 he was a Research Assistant and held a CRES Fellowship at the Center for Research in Engineering Sciences, University of Kansas. He conducted research concerned with electromagnetic wave propagation and the optimization and synthesis techniques of antenna arrays. In 1965, he joined the faculty of the School of Engineering and Applied Science, Southern Methodist University, Dallas, TX where he is now Professor and Chair of Electrical Engineering and a University Distinguished Professor. His primary research areas are solid state injection lasers, radiation and detection studies of lasers, millimeter wave communication and fiber optic systems, integrated optics and the application of integrated optical circuits, and quantum electronics.

In 1977 Dr. Butler was given the Southern Methodist University Sigma Xi Research Award. In the summers since 1969, he has been a Staff Scientist, David Sarnoff Research Center (formerly RCA Laboratories), Princeton, NJ. He has held consulting appointments with the Central Research Laboratory of Texas Instruments, Inc., the Geotechnical Corporation of Teledyne, Inc., Earl Cullum Associates of Dallas, TX and the University of California Los Alamos Scientific Laboratory, Los Alamos, NM. He was elected a Fellow of IEEE for contributions to semiconductor lasers and the theory of radiation characteristics of optical waveguides. He is a member of Sigma Xi, Tau Beta Pi, Eta Kappa Nu, and a Registered Professional Engineer in the State of Texas.

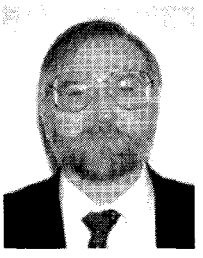

Gary A. Evans (S'69–M'75–SM'82–F'92) was born in Omak, WA. He received the B.S.E.E. degree from the University of Washington, Seattle, in 1970, and the M.S.E.E. and Ph.D. degrees in electrical engineering and physics from the California Institute of Technology, Pasadena, in 1971 and 1975.

After post-doctoral work at Caltech, he worked for R&D Associates, Marina Del Rey, CA, and was a Visiting Assistant Professor in the Electrical Engineering Department at the University of Washington. He has worked at the Aerospace Corporation, El Segundo, CA, TRW, Redondo Beach, CA, and RCA Laboratories (now the David Sarnoff Research Center), Princeton, NJ. In 1992 he joined Southern Methodist University as a Professor in the Electrical Engineering Department. Since 1979 he has primarily worked on the design, growth, and fabrication of conventional cleaved facet and grating surface emitting semiconductor lasers.

Dr. Evans was elected a Fellow of the IEEE for "contributions to the development, fabrication, and understanding of semiconductor lasers," has over 170 publications, and is a co-editor of the Academic Press book *Surface Emitting Semiconductor Lasers.* He is a Licensed Professional Engineer, has served on numerous IEEE committees, is a past Chairman of the Princeton Lasers and Electro-Optics Society (LEOS) Section, a past Chairman of the Santa Monica Bay Section of the IEEE, and was an Associate Editor of the IEEE JOURNAL OF QUANTUM ELECTRONICS.

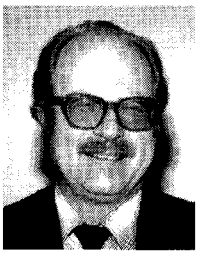

Arye Rosen (M'77–SM'80–F'92) received the M.Sc.E. degree from Johns Hopkins University, the M.Sc. degree in physiology from Jefferson Medical College, and the Ph.D. degree in electrical engineering from Drexel University.

He is a Senior Member of the Technical Staff at the David Sarnoff Research Center (formerly RCA Laboratories) in Princeton, NJ, which he joined in 1967 and where he is currently responsible for research and development in the areas of millimeter wave devices and circuits and microwave optical interaction. The author of more than 150 technical papers, he is co-editor of *High-Power Optically Activated Solid-State Switches*, (Boston, MA: Artech House, 1993), and of *New Frontiers in Medical Device Technology* (New York: Wiley, 1995). He holds 45 U.S. patents in the fields of engineering and medicine.

Dr. Rosen is the recipient of numerous Achievement and Professional Awards, including a 1989 IEEE Region One Award, "for significant contributions to microwave technology by the invention and development of Microwave Balloon Angioplasty." He is a Fellow of the IEEE, a member of the IEEE MTT-S Technical Program Committee since 1979, MTT-S Technical Committee Chairman on Biological Effects and Medical Applications, Associate Editor of the IEEE JOURNAL OF LIGHTWAVE TECHNOLOGY (JLT), and a member of the Editorial Board of Microwave and Optical Technology Letters. He has served on the Technical Committee for the IEEE International Conference on Microwaves in Medicine held in Belgrade, Yugoslavia, in April 1991. He is also a Member-at-Large of the IEEE Health Care Engineering Policy Committee, and a Member of the IEEE Educational Activities Board. His biography has been selected for inclusion in *Marquis Who's Who In The World* 1995–1996.